Cas9 fusions for precision *in vivo* editing

Ryan R. Richardson, Marilyn Steyert, Jeffrey Inen, Saovleak Khim, Andrea J. Romanowski, Bekir Altas, Alexandros Poulopoulos

Department of Pharmacology, University of Maryland School of Medicine, Baltimore, MD, USA

Corresponding author: AP, apoulopoulos@som.umaryland.edu
670 W Baltimore St, HSF3-9178, Baltimore, MD, 21201, USA

Abstract

Current Cas9 reagents can target genomic loci with high specificity. However, when used for knockin, on-target outcomes are inherently imprecise, often leading to unintended knockout rather than intended edits. This restricts applications of genome editing to *ex vivo* approaches, where clonal selection is possible. Here we describe a workflow using iterative high-throughput *in vitro* and high-yield *in vivo* assays to evaluate and compare the performance of CRISPR knockin reagents for both editing efficiency and precision. We tested combinations of Cas9 and DNA donor template variants and determined that Cas9-CtIP with *in situ* linearized donors display fold-increases of editing precision in cell lines and *in vivo* in the mouse brain. Iterating this process, we generated novel compound fusions, including eRad18-Cas9-CtIP that showed further fold-increases in performance. Continued development of precision editing reagents with this platform holds promise for direct *in vivo* knockin across model organisms and future targeted gene therapies.

Introduction

The CRISPR toolkit has brought into sight the prospect of direct genome manipulation within intact organisms. This prospect, and how well it is realized, will determine the impact of the genome editing revolution in both biological research and biomedical therapeutics. Conventional multi-generational, resource-intensive, and species-specific knockin technologies present practical barriers to entry for experimentation. This often relegates knockin approaches to formulaic *in vivo* confirmations for discoveries made in more versatile *in vitro* systems. Future cost- and time-effective alternative knockin approaches would facilitate and expand genome-enabled exploratory research directly *in vivo*.

The continued development of new CRISPR reagents with improved performance holds promise for achieving precise and efficient direct knockin of target cells in wild-type organisms. This would drastically lower the resource burden and turnover time for experiments in which targeted manipulations are made directly onto endogenous genes within their native *in vivo* context. The broad efficacy of Cas9 across biological systems promises that such approaches will overcome the pronounced species disparities in access to genetic engineering technologies, opening up biological experimentation into previously genome-challenged model organisms that are otherwise experimentally advantageous. This breadth of application includes the promise of direct *in vivo* editing in humans, which if precise enough, would enable *in situ* gene therapeutics beyond the select systems currently amenable to *ex vivo* editing approaches[1].

Current Cas9-based knockin methods produce the desired editing outcome the minority of the time, with their most frequent outcomes being unintended on-target indels. Such low efficiency and imprecise knockin is only useful when paired with subsequent clonal selection, verification, and expansion of correctly edited cells. This has found practice in editing stem cells from which can be derived cell and animal lines. In gene therapy, while Cas9-based knockin performs below therapeutic values[2], it has found practice in *ex vivo* editing therapies. In these approaches, cells are extracted from the patient, edited *in vitro*, selected, verified, expanded, and then transplanted back into the patient[3]. These methods require cells to be mitotic or reprogramed to allow for clonal selection and expansion. If *in vivo* gene editing were precise enough, it would offer direct *in situ* gene therapy alternatives in cases where cell transplantation is not feasible, particularly in tissues with highly structured cellular connectivity, such as the brain[4,5], the retina[6,7] and the heart[8].

In vivo knockin with Cas9 is already finding use, despite its low efficiency and precision, in tagging endogenous proteins for sparse labeling[9,10,11,12]. These approaches rely on selectively identifying correctly edited alleles through visualizing the expression of a knockin tag. These approaches enable endogenous protein tagging with sparse labeling, and have the advantage of polyclonal editing that minimizes potential off-target clonal artifacts. The major caveats of such approaches are that high rates of unintended on-target indels often lead to unintended and undetected knockout

of the second allele in knockin labeled cells, introducing potential dark haploinsufficiencies that confound interpretations.

Toward the development of high-performance Cas9-based reagents for direct *in vivo* knockin, here we present an experimental workflow pairing high-throughput *in vitro* characterization with high-yield *in vivo* testing to comparatively assess both efficiency and precision metrics of editing outcomes. Using a florescence-based editing assay, we screened a matrix of existing Cas9 variant and DNA donor template combinations, revealing that *in situ* linearized dsDNA donors with Cas9 fused to a fragment of the DNA repair protein CtIP[13] significantly improved both knockin efficiency and precision. Select reagents were evaluated with *in utero* electroporation into the mouse brain, corroborating fold-improvements in editing performance *in vivo*. Iteration of this workflow with novel variants of the top performers fused to DNA repair proteins, such as eRad18 and Rad52, led to further improvements in knockin precision. These data demonstrate the potential of the generalizable workflow for the continued development and assessment of new *in vivo* genome editing reagents, toward precision knockin reagents to facilitate *in vivo* research models and new therapeutics for genetic disease.

Methods

Plasmid design and construction

Mammalian expression plasmids and knockin donor template plasmids were constructed with a combination of standard cloning techniques. For sgRNA expression constructs, oligos (Integrated DNA Technologies) were annealed and cloned into a custom hU6 backbone using Golden Gate Assembly (GGA)[14]. Cas9 expression constructs were assembled by a modified mMoClo system[15]. Briefly, individual parts were cloned, BsaI adapters added, and internal sites removed via PCR using KAPA HiFi HotStart DNA Polymerase with 2X Master Mix (Roche), or synthesized (Integrated DNA Technologies). Parts were subsequently assembled into expression constructs using NEB Golden Gate Assembly Kit (BsaI-HF v2) according to manufacturer's recommendations. Homology arms for donor templates were PCR amplified from CD1 mouse genomic DNA with adapters for GGA. sgRNA binding site (GRBS) parts were generated by oligo annealing. GRBS and homology arms were assembled with knockin sequences via GGA. See Supplemental Table 1 for further detail.

Cell lines and Culture

HEK:BFP cells were the kind gift of Chris Richardson[16]. N2A cells were the kind gift of Peter Crino (University of Maryland School of Medicine, Baltimore, MD). HEK:BFP and N2A cells were maintained at 37°C and 5% CO2 in DMEM media plus GlutaMax (ThermoFisher Scientific) supplemented with 10% (v/v) fetal bovine serum (FBS). NIH/3T3 ('3T3', ATCC CRL-1658TM) were maintained at 37°C and 5% CO2 in DMEM media plus GlutaMax supplemented with 20% FBS.

Mammalian cell transfection

Typically, 20,000-22,500 cells/cm2 were seeded onto 24-well plates the day before transfection, and were roughly 70-80% confluent at the time of transfection. For N2A and 3T3 cells, plates were pre-coated with poly-L-lysine (Sigma-aldrich). HEK:BFP and N2A cells were transiently transfected using Polyethylenimine, Linear, MW 25000 ('PEI', Polysciences)

resuspended to 1mg/mL in H2O at a 3:1 (v/w) PEI:DNA ratio. 3T3 cells were transfected with Transfex Transfection Reagent (ATCC ACS-4005TM) at a 3:1 (v/w) PEI:DNA ratio. 250 ng DNA per plasmid was transfected for a total of 500 ng or 750 ng DNA per well, with empty vector used to maintain the total amount of DNA constant across transfection conditions. Transfection reagent (PEI or Transfex) was diluted in 25 µl Opti-MEM (ThermoFisher Scientific) and incubated for 5 minutes at room temperature. DNA diluted in 25 µl Opti-MEM was then mixed with the diluted transfection reagent and incubated for a further 15 minutes before being added dropwise to cells.

Flow cytometry

Cells were trypsinized, pelleted, and resuspended in Dulbecco's PBS containing 0.1% FBS. At least 20,000 live cells (typically 80,000+) were analyzed using an LSRII cell analyzer with HTS (BD Biosciences). EBFP and mTagBFP were measured with a 407 nm laser and a 450/50 emission filter. EGFP and mNeonGreen were measured with a 488 nm laser, a 505 LP mirror, and a 530/30 emission filter. mCherry was measured with a 561 nm laser, a 600 LP mirror, and a 615/25 emission filter. Data were analyzed with FlowJo v10.6.2 (Flowjo LLC). Live cells were gated by size and granularity using FSC-A vs SSC-A. Singlets were gated using SSC-A vs SSC-H (see Supplementary Fig. 1). At least 3 biological replicates were run with internal technical duplicates or triplicates.

Sequence analysis of knockin products

Transiently transfected HEK:BFP cells were sorted using a FACSAria II sorter (BD Biosciences). Genomic DNA was extracted from sorted cells using the Genomic DNA Clean & Concentrator kit (Zymo Research). PCR fragments were amplified using KAPA HiFi HotStart DNA Polymerase with 2X Master Mix (Roche), gel extracted with Zymoclean Gel DNA Recovery kit (Zymo Research), and submitted for Sanger sequencing (Genewiz). See Supplementary table 1 for primer sequences. Alignment of sequencing results was performed using Benchling (https://benchling.com). Analysis of editing outcomes by decomposition of Sanger sequencing data was performed using the ICE Analysis tool v2 (Synthego) as previously described[17].

Animals

All animal experimental protocols were approved by the University of Maryland Baltimore Institutional Animal Care and Use Committee and complied with all relevant ethical regulations regarding animal research. Experiments were performed on outbred strain CD1 mouse pups (Charles River Laboratories). Analyses are thought to include animals of both sexes at approximately equal proportions, as no sex determination was attempted. No statistical methods were used to predetermine sample size.

In utero electroporation

Electroporations of plasmid DNA were performed in utero on embryonic day 14.5 (E14.5) to target cortical layer II/III, as previously described[1819]. Briefly, DNA solutions were prepared to 4 µg/µL total DNA, with 1 µg/µL of each of the relevant plasmids (donor, guide, Cas9, and electroporation control). Dames were deeply anesthetized with isoflurane under a vaporizer thermal support with (Patterson Scientific Link7 & Heat Therapy Pump HTP-1500). The abdominal area was prepared for surgery with hair removal and surgical scrub. Exposed skin was wiped with 70% ethanol and 10% Betadine solution. A midline incision was created in the skin and abdominal muscle layers to expose the uterine horns. Using pulled (Narishige PC-100) and beveled (Narishige EG-45) glass micropipettes connected to a pneumatic aspirator, DNA solution was injected into one lateral brain ventricle of each fetus, followed immediately by application of 4 x 50 ms square pulses of 35 V (NEPA21 electro-kinetic platinum tweezertrodes connected to a BTX ECM-830 electroporator) targeting nascent sensorimotor areas of the

cortical plate. Typically, 4-6 pups were electroporated per dame. Uterine horns were placed back inside the abdominal cavity, and monofilament nylon sutures (AngioTech) were used to close both muscle and skin incisions. After term birth, electroporated mouse pups were non-invasively screened for unilateral cortical fluorescence using a fluorescence stereoscope (Leica MZ10f with X-Cite FIRE LED light source) and returned to their dame until postnatal day 7 (P7). When possible, to minimize inter-dame variation, control and experimental electroporations were performed in littermate pups from the same dame.

Histology and immunolabeling

Tissue was prepared by intracardial perfusion with PBS and 4% paraformaldehyde. Brains were cut to 80 µm coronal sections on a vibrating microtome (Leica). For immunolabeling, slices were incubated in blocking solution consisting of 5% bovine serum albumin and 0.2% Triton X-100 in PBS for 30 minutes, then incubated overnight at 4°C with primary antibodies diluted in blocking solution. The next day, sections were washed three times in PBS, then incubated for 3 hours at room temperature with secondary antibodies diluted 1:1000 in blocking solution. Following three PBS washes, sections were mounted on slides with Fluoromount-G Mounting Medium with DAPI (ThermoFisher Scientific). See Supplementary Table 1 for details on specific antibodies.

Microscopy and image analysis

Fluorescence images were acquired using a Nikon Ti2-E inverted epifluorescence microscope fitted with an automated registered linear motor stage (HLD117, Pior Scientific), a Spectra-X 7 channel LED light engine (Lumencor), and standard filter sets for DAPI, FITC, TRITC, and Cy5. Images were analyzed with NIS-Elements (Nikon) using an automated script to identify and count electroporated cells in brain sections. Knockin, mCherry-positive neurons were counted manually using ImageJ (NIH) and independently by three blinded investigators. Five 80 µm sections, centered at the middle of the anteroposterior axis of the electroporation field and taken every other section, were analyzed per brain, with counts aggregated across sections from the same brain.

Statistical analysis

All statistical values are presented as mean ± SEM. For experiments containing more than two conditionals or groups, statistical significance was calculated using a one-way ANOVA with Tukey's multiple comparison test, with a single pooled variance. For experiments containing two conditionals or groups, statistical significance was calculated using a two-tailed Student's T test. Differences between conditions were judged to be significant at $P < 0.05$ (*), $P < 0.01$ (**), and $P < 0.001$ (***). See Supplementary Information for full details on statistical analyses.

Results

Combinatorial screening of CRISPR knockin components for improved efficiency and precision

To identify elements in CRISPR knockin reagents that offer improved efficiency and precision, we investigated combinations of three variables, for which reagent variants are available that have individually been shown to enhance knockin performance. We compared i) wildtype SpCas9 ('WT') versus a High-Fidelity ('HF') sequence variant (SpCas9-HF1)[20,21]; ii) Cas9 variants alone versus fusions with a fragment of the DNA repair protein CtIP[13]; iii) knockin donor on circular DNA predicted to favor homologous recombination ('HR') vs. linear DNA

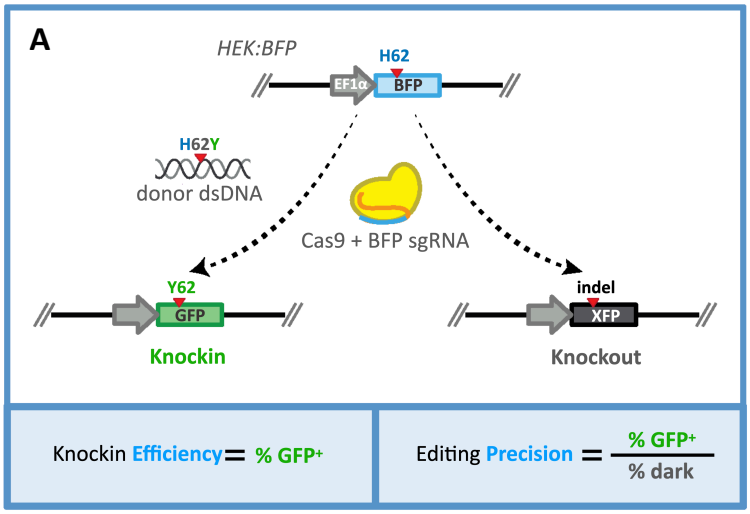

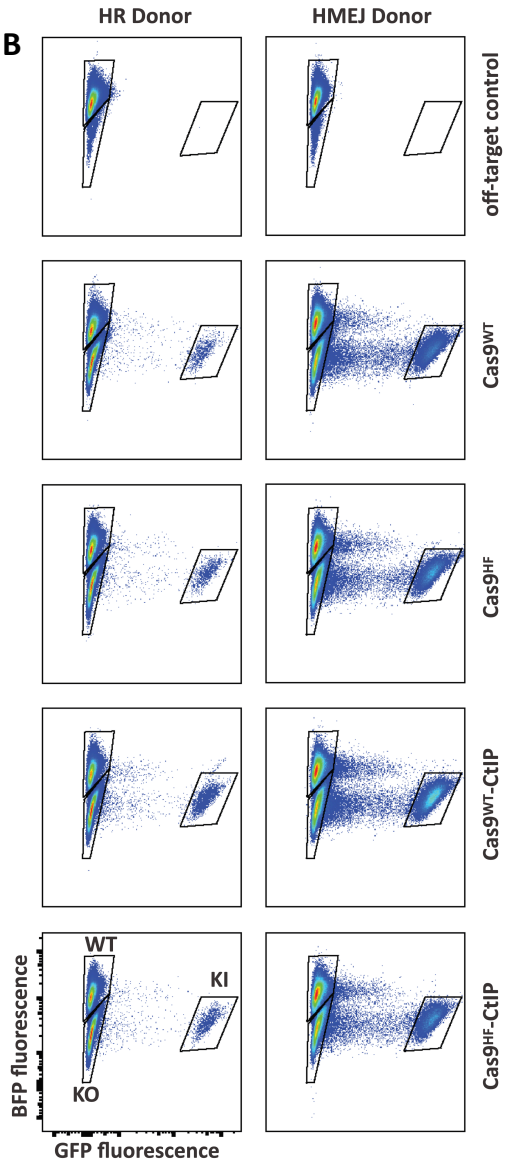

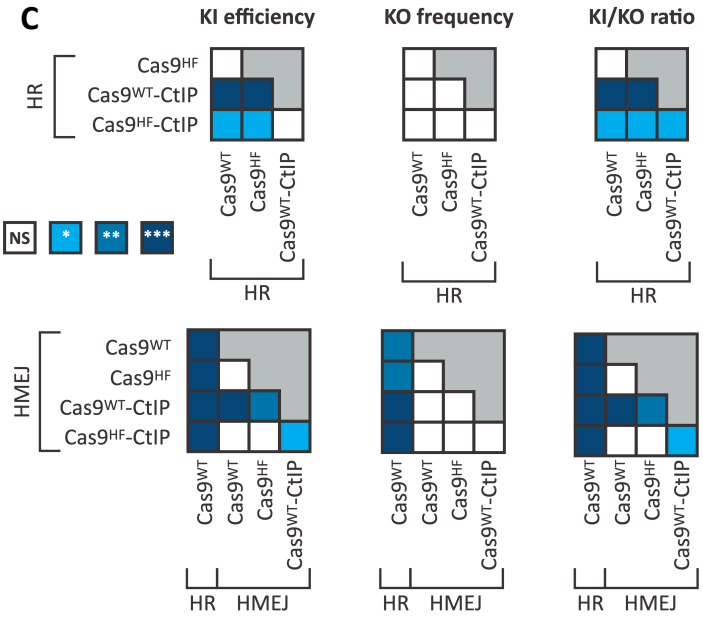

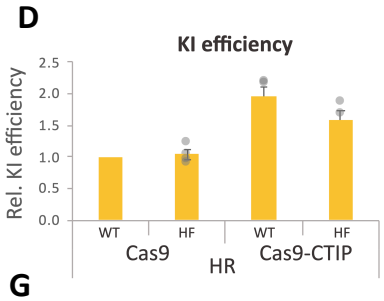

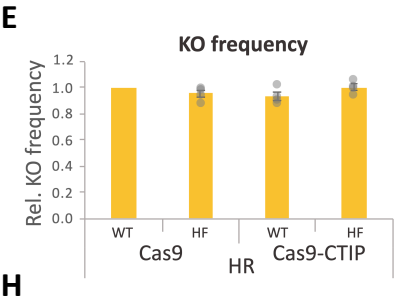

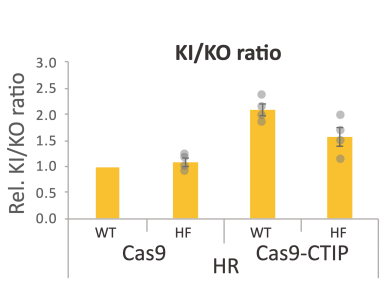

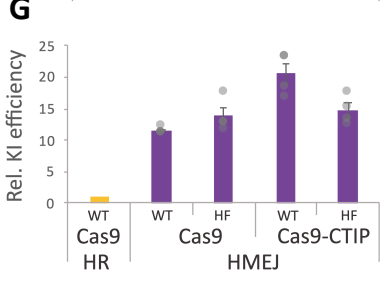

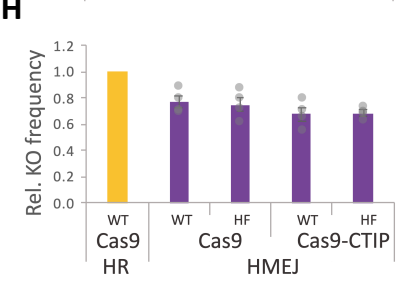

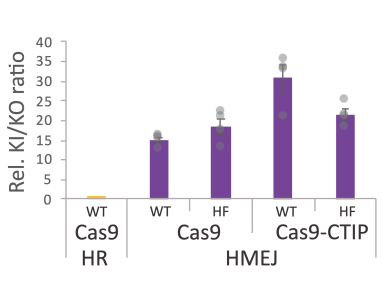

Fig. 1. CtIP fusion and HMEJ donors additively improve knockin-to-knockout ratio (KI/KO). **(A)** Schematic of BFP to GFP conversion assay in HEK293 cells. Gene editing of the genomic BFP gene can result in GFP expression, indicative of knockin, or loss of fluorescence, indicating knockout. This fluorescence readout is used to calculate knockin efficiency and precision. **(B)** Flow cytometry plots of HEK:BFP cells 7 days after transient transfection with sgRNA, Cas9, and donor. **(C-I)** Quantification of flow data representing normalized **(D)** knockin efficiency (%GFP+), **(E)** knockout frequency (%BFP-), and **(F)** KI/KO ratio for HR donor and Cas9 variants. **(G-H)** Quantification of respective values with HMEJ donor and Cas9 variants. Mean values from individual experiments ($n \geq 3$) were normalized to those of the $Cas9^{WT}$ with HR donor condition and presented as the mean ± SEM. **(C)** Heatmaps displaying statistical significance calculated using a one-way ANOVA with Tukey's multiple comparison test, with a single pooled variance (* $P<0.05$; ** $P<0.01$; *** $P < 0.001$).

predicted to favor homology-mediated end joining ('HMEJ'). Both knockin donors were provided on a plasmid with the knockin sequence flanked by ~800bp homology arms, the length of which did not significantly affect results within a window of 500 to 1500 bp (data not shown). The HMEJ donor differed from the HR donor by the insertion of sgRNA Binding Sites (GRBS) flanking the homology arms, that are cleaved by Cas9 *in situ* to create linear dsDNA donors in cells. The orientation of the GRBSs did not have significant effects on editing performance (Supplementary Fig. 3).

To quantify the effects of these Cas9 and donor variant combinations on knockin efficiency, we used an *in vitro* BFP to GFP conversion assay in an engineered HEK293 cell line (HEK:BFP) stably expressing BFP[16]. Here, donors are designed to target the genomic BFP sequence and convert it to GFP via introduction of the point mutation H26Y. Following transfection of these cells with Cas9, sgRNA targeting BFP, and H26Y donor template, flow cytometry was used to quantify the resulting changes in fluorescence (Fig. 1A). As on-target insertions or deletions of the BFP ORF by error-prone double-strand break (DSB) repair often leads to disruptive frameshift mutations, loss of fluorescence is a good surrogate for quantifying the incidence of gene KO (see below and Fig. 2C). In this manner, precise H26Y knockin is represented by the spectral shift from BFP to GFP, while unintended knockout by loss of fluorescence. By quantifying the proportions of BFP, GFP, and dark cells, we ratiometrically assessed knockin efficiency (ratio of GFP to BFP cells) and knockin precision (ratio of GFP to dark cells) in the matrix of Cas9 and knockin donor variants.

While transfection of the off-target control sgRNA resulted in no GFP expression, transfection with the BFP sgRNA led to increases in both the knockin (BFP-/GFP+) and knockout (BFP-/GFP-) populations for all combinations of donors and Cas9 variants (Fig. 1B). Consistent with previous reports[13,22,23], among the Cas9 variants, $Cas9^{WT}$-CtIP performed with a roughly 2-fold improvement in knockin efficiency compared to $Cas9^{WT}$, regardless of donor variant (Fig. 1D, 1G). $Cas9^{HF}$ variants were generally not significantly different from $Cas9^{WT}$, although $Cas9^{HF}$-CtIP showed a 1.6-fold improvement in knockin efficiency specifically with the HR donor. Interestingly, KO rates did not significantly differ among the Cas9 variants, and thus, the KI/KO ratio for the HR donor mirrors the differences seen in knockin efficiency (Fig. 1E, 1F).

In contrast to the Cas9 variants, donor architecture impacted not only knockin efficiency but also knockout rate (Fig. 1G, 1H). Across all four Cas9 variants, the HMEJ donor showed a 9- to 13-fold increase in knockin efficiency. Of the combinations of Cas9 and donor, $Cas9^{WT}$-CtIP in conjunction with the HMEJ donor resulted in the highest rate of knockin, 24-fold higher than $Cas9^{WT}$ with the HR donor. Regardless of Cas9 variant, the HMEJ donor showed a 22-30% reduction in gene disruption, which, together with the improvement in knockin efficiency, enhanced the KI/KO ratio by about 15-fold relative to the HR donor template permutations (Fig. 1I and Supplementary Fig. 2). Interestingly, these data suggest the independent and additive

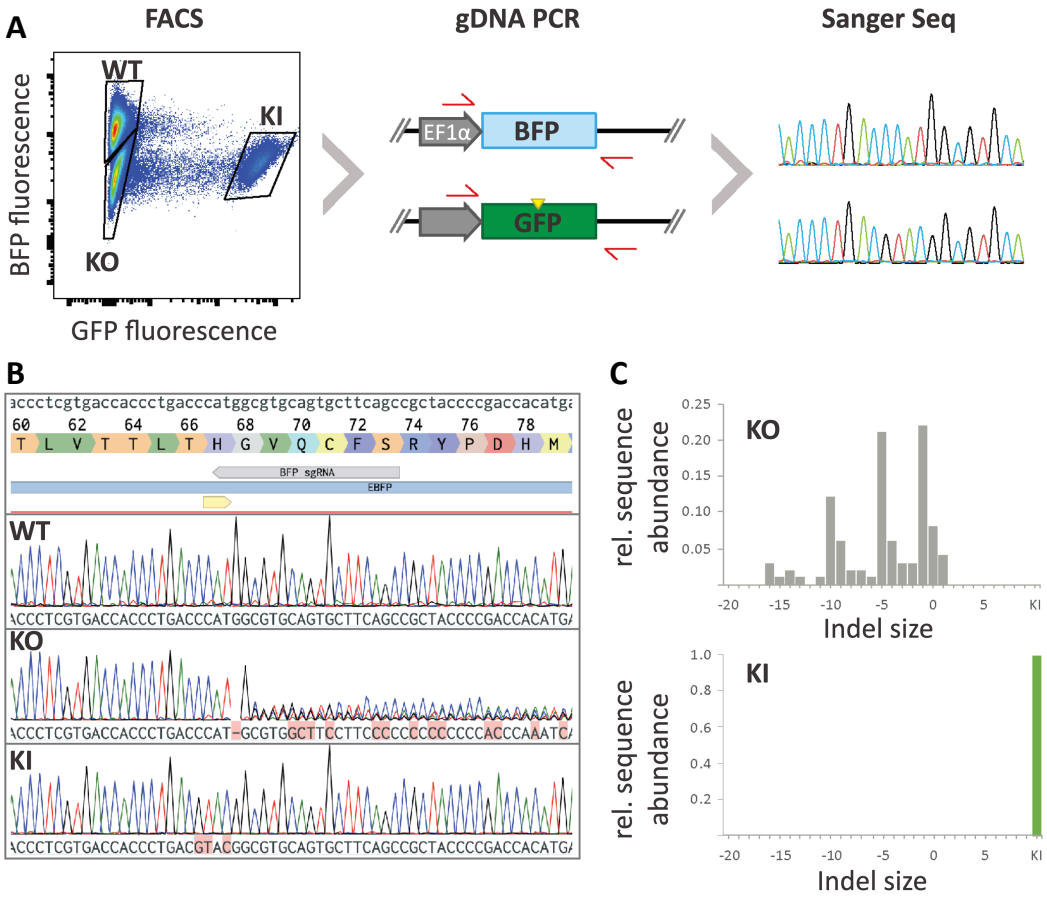

Fig. 2. CtIP fusion and HMEJ donor yield high-performance knockin. **(A)** Schematic outlining FACS isolation of distinct cell populations following gene editing with Cas9^{WT}-CtIP and HMEJ donor, genotyping PCR of the target genomic DNA (gDNA) locus, and Sanger sequencing of the amplified fragment pool. **(B)** Alignment of Sanger sequencing reads for wild-type, knockout, and knockin populations to the reference template (top). **(C)** Editing outcomes (indels, knockin frequency) were quantified by decomposition of Sanger sequencing reads using the ICE algorithm and plotted in histograms binned by indel size.

contributions of both CtIP fusion (~2-fold) and the *in situ* linearization of HMEJ donors (~11-fold) to KI efficiency. Taken together, these results demonstrate that combinatorial optimization of both Cas9 and the donor DNA can significantly shift the balance of DSB repair, with the combination of Cas9^{WT}-CtIP and HMEJ donors giving the highest efficiency and precision in HEK293 cells.

High-performance knockin with CtIP fusion and HMEJ donor

Imperfect integration of donor DNA at the targeted genomic locus can result in unintended disruptions in gene function[24]. To investigate the fidelity of fluorescence-based readouts to gene editing genotype, we FACS sorted Wt (BFP+/GFP-), KO (BFP-/GFP-), and KI (BFP-/GFP+) populations of HEK:BFP cells following transfection with Cas9^{WT}-CtIP and HMEJ donor (Fig. 2A). Genomic DNA was extracted from sorted cell populations and used as template in PCR with primers flanking the region targeted by Cas9 in the BFP locus, thereby amplifying all alleles regardless of editing outcome. Each sorted cell population gave rise to a pool of PCR fragments that was then analyzed by Sanger sequencing. As expected, the genotype of the

WT population exactly matched that of the reference BFP template (Fig. 2B). The KO population on the other hand, showed a complex mixture of genotypes clustered near the cleavage site for the BFP sgRNA representing unintended on-target edits. Finally, the KI population appeared to have a single genotype containing only the desired edits from the donor template.

As these Sanger data were from mixtures of cells and not isolated clones, we performed sequencing decomposition using the ICE algorithm[25] to get a more specific and quantitative assessment of editing outcomes for the KI and KO populations (Fig. 2C). ICE results for the KO population show a predominance of indels predicted to cause a frameshift mutation (79% frameshift vs 11% in-frame), in line with the observed loss of BFP in this population. In contrast, sequence decomposition for the KI population displayed a single genotype corresponding to the desired GFP edit. Together, these sequencing data corroborate the fluorescence-based editing readouts and confirm that CtIP fusion combined with HMEJ donor plasmid result in high-performance knockin that faithfully introduces intended edits.

CtIP fusion increases knockin efficiency *in vivo*

Following the dramatic increase in knockin efficiency and precision seen *in vitro* with the combination of Cas9^{WT}-CtIP and HMEJ donor, we sought to validate these reagents for efficacy *in vivo*. To test *in vivo* knockin efficiency, we used an *in utero* electroporation model targeting integration of a 2A mCherry cassette to the β-Actin (*ActB*) locus of wild-type mice (Fig. 3A). Cas9 and donor variants, along with *ActB* sgRNA and a GFP transfection marker, were electroporated into embryonic day 14.5 (e14.5) pups targeting progenitors of sensorimotor cortex layer II/III neurons. knockin efficiency in neurons was calculated at postnatal day 7 (P7) by comparing the number of mCherry-positive knockin neurons to the total number of electroporated, GFP-positive neurons (Fig. 3B). Electroporation of the standard Cas9 and HR donor resulted in a 10.3 ± 2.2% knockin rate (Fig. 3C). Substitution of the Cas9-CtIP fusion yielded 26.0 ± 5.1% KI efficiency. Surprisingly, irrespective of Cas9 variant, *in vivo* editing with the HMEJ donor led to a similar level of knockin compared to the uncleaved HR donor, 8.0 ± 2.6% with Cas9 alone and 19.6 ± 4.7% with Cas9-CtIP, respectively.

Contrary to the *in vitro* results showing a 10-fold improvement in knockin efficiency with HMEJ donors, these data suggest that HMEJ donors do not enhance *in vivo* knockin performance in the embryonic mouse brain. However, CtIP fusion to Cas9 led to 2.4-fold higher rate of knockin compared to Cas9 alone, in line with *in vitro* data (Fig. 3D). Ultimately, while these results show significant improvements in knockin efficiency, they also highlight the need for further optimizations in knockin performance *in vivo*.

Compound Cas9-CtIP fusions with eRad18 and Rad52 improve editing precision

Several groups have independently demonstrated that modulation of DNA repair pathways is an effective way to improve knockin efficacy and precision[26,13,23,27,28]. To further improve on the *in vivo* results using CtIP-fused Cas9, we returned to the *in vitro* BFP-to-GFP conversion assay with an HMEJ donor, and evaluated the impact of five DNA repair proteins (dn53BP1, TIP60, RNF169, Rad52, eRad18) on editing efficiency and precision when fused N-terminally to Cas9 or Cas9-CtIP (Fig. 4). In the absence of CtIP, only eRad18 fusion to Cas9 significantly improved knockin efficiency, increasing it by 1.8-fold above Cas9^{WT} alone, comparable to the effect of C-terminal CtIP fusion to Cas9^{WT} (Fig. 4A). While compound fusion of dn53BP1, TIP60, or RNF169 to Cas9^{WT}-CtIP appeared to abrogate the effect of CtIP on KI efficiency, the addition of Rad52 or eRad18 did not have a detrimental impact on efficiency.

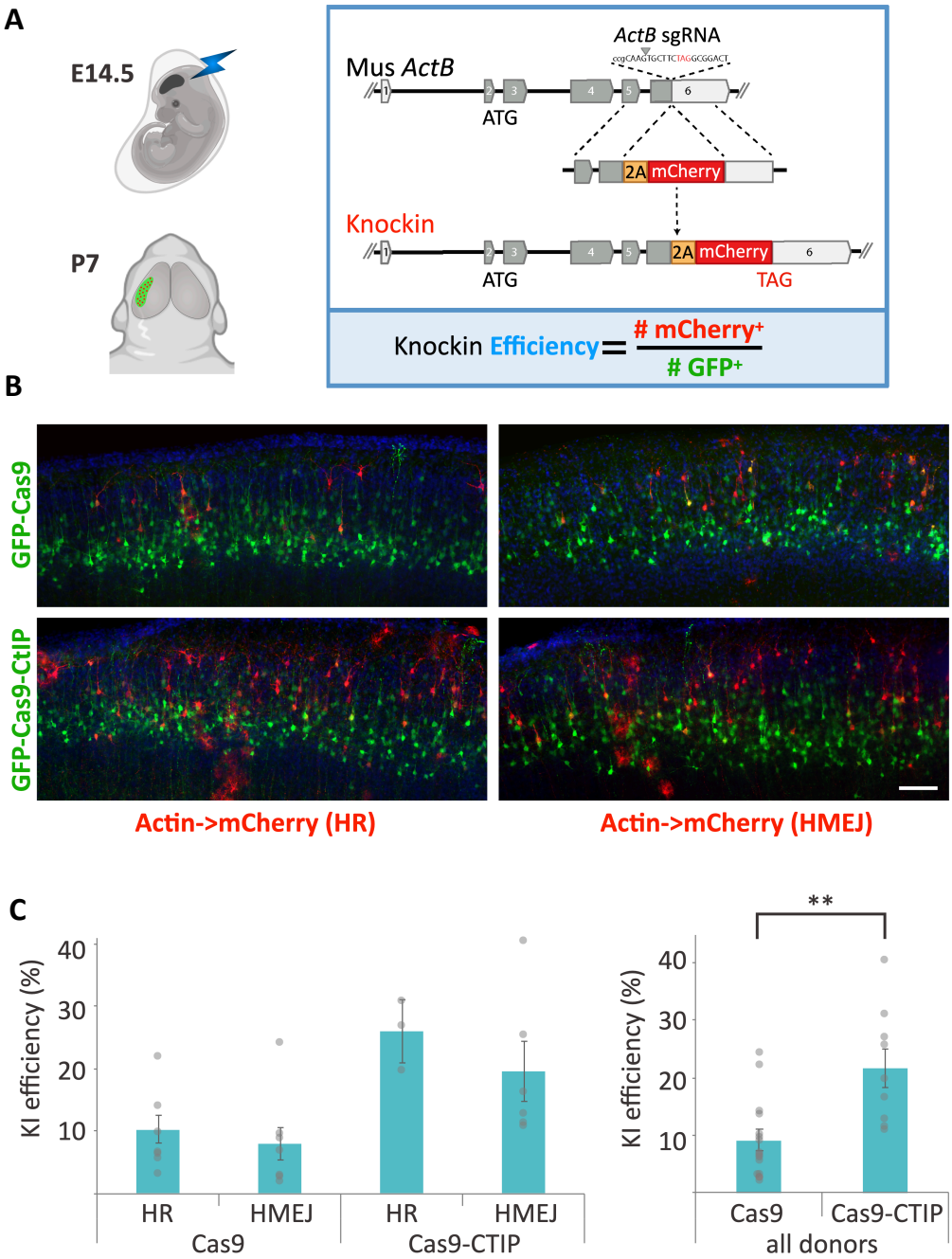

Fig. 3. CtIP-fusion improves knockin efficiency *in vivo*. **(A)** Schematic of *in vivo* editing strategy using *in utero* electroporation in the fetal brain at E14.5, and analysis at P7. Gene editing of the endogenous *ActB* locus results in mCherry expression, indicating knockin. Along with a GFP transfection marker, this fluorescence readout is used to calculate KI efficiency. **(B)** Fluorescence images of the cerebral cortex with electroporated neurons receiving Cas9 or Cas9-CtIP and HR or HMEJ donor variants). Images show nuclear DAPI (blue), plasmid GFP (green) and knockin mCherry (red). **(C-D)** Bar graphs showing quantification of *in vivo* knockin efficiency for **(C)** Cas9 and donor variants, and **(D)** aggregate Cas9 vs Cas9-CtIP with all donors. Values are presented as the mean ± SEM. For (D), statistical significance was calculated using a two-tailed Student's T test. Differences between conditions were judged to be significant at $P < 0.01$ (**).

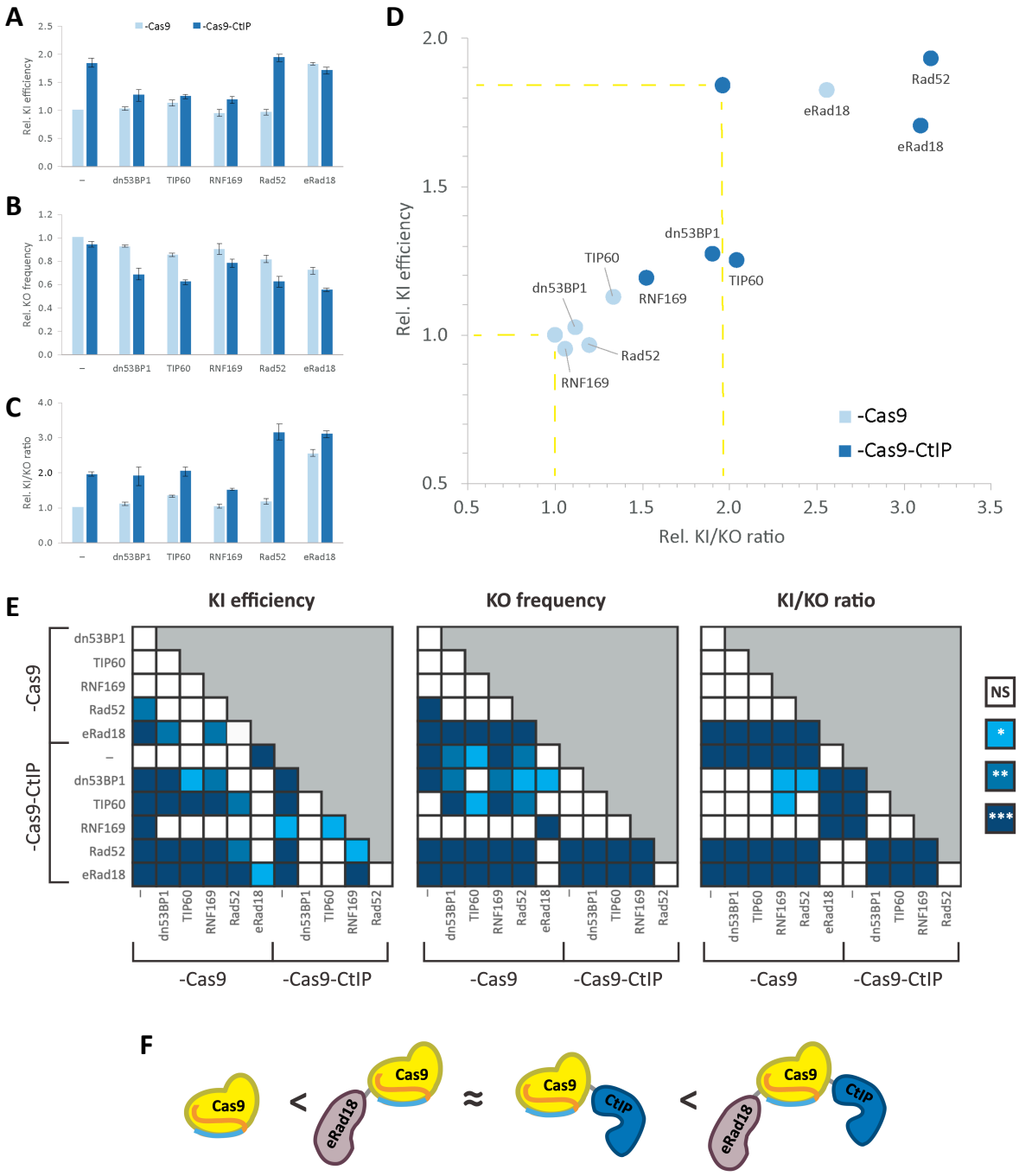

Fig. 4. Additional DNA-repair protein fusions can improve precision editing of Cas9 and Cas9-CtIP. **(A-C)** Bar graphs showing quantification of **(A)** relative knockin efficiency, **(B)** knockout frequency, and **(C)** KI/KO ratio for HEK:BFP cells transiently transfected with BFP sgRNA, GFP HMEJ donor, and Cas9^{WT} or Cas9^{WT}-CtIP fused to the listed DNA-repair proteins. Values from individual experiments ($n \geq 3$) were normalized to the Cas9^{WT}-only condition and presented as the mean ± SEM. **(D)** Scatter plot correlating knockin efficiency and KI/KO ratio. **(E)** Heatmap showing statistical significance calculated using a one-way ANOVA with Tukey's multiple comparison test, with a single pooled variance (* $P<0.05$; ** $P<0.01$; *** $P < 0.001$). Data of replicate experiments are shown in Supplementary Fig. 6. **(F)** Schema illustrating comparative performance of novel fusions eRad18-Cas9 and eRad18-Cas9-CtIP compared to parent proteins.

Regarding knockout, dn53BP1-, TIP60-, and RNF169-fused Cas9^{WT} did not significantly differ from the Cas9-only control (Fig. 4B). Rad52 and eRad18 fusion, however, showed 18% and 28% reductions in knockout frequency, respectively. Interestingly, compound fusion of each of the five DNA repair proteins with CtIP led to significant reductions in the knockout rate, with eRad18, Rad52, and TIP60 showing the most pronounced decreases (45%, 38% and 38%, respectively). Despite these reductions in knockout rates, only Rad52 and eRad18 led to significant improvements in overall knockin precision (Fig. 4C). Without CtIP, eRad18 demonstrated a 2.5-fold increase in the knockin-to-knockout ratio, while combination of either Rad52 or eRad18 with CtIP led to a 3.1-fold increase in precision relative to Cas9^{WT} alone. These results show that specific combinations of DNA repair molecules can function together to improve both the efficiency and precision of Cas9-mediated KI.

Discussion

In vivo application of genome editing technologies offers tremendous potential for developing better animal models and for therapeutic benefit in humans. To realize this potential, new reagents need to be developed with significant improvements in performance metrics. Many systems are currently available with adequate performance for knockin *in vitro*, where modified cells can be selected for and expanded as single clone-derived populations. For direct *in vivo* editing to be broadly practicable, its performance must achieve both high on-target efficacy and low rates of unintended outcomes. Toward the development of such high-performance editing reagents, in this study, we explored variants of Cas9, DNA repair proteins, and DNA donor templates, and identified novel combinations that resulted in high-performance knockin with fold-improvements in editing efficiency and precision.

When paired with an *in situ* linearized dsDNA donor, fusion of CtIP to wild-type Cas9 led to a 20-fold increase in knockin efficiency and 30-fold increase in editing precision (Fig. 1G, 1I). Interestingly, our data indicate independent and additive contributions from both the CtIP fusion (approximately 2-fold increase) and the linear HMEJ donor (over 10-fold increase) to knockin efficiency, as well as an independent effect of the HMEJ donor on reducing knockout by over 25% (Fig. 1 and Supplementary Fig. 2). The individual increases in efficiency mirror previous studies[13,29], however their cumulative efficacy and the reduction of knockout rates has not been previously demonstrated.

The independence of CtIP and HMEJ donor effects suggests that these two optimizations function through different, parallel mechanisms. Indeed, while the role of CtIP in multiple homology-mediated repair pathways is well characterized, it has been speculated that linear donors may also function through a number of different repair pathways[30,23,31,29]. Difference in DNA repair pathway utilization across cell types and developmental stages may underly the quantitative variability in knockin efficiencies observed across host cell types assayed in this study, and underscores the challenge in translating *in vitro* results to *in vivo* application.

The observation of cumulative improvements on editing performance prompted us to further iterate the screening workflow to build upon the best performer of the previous cycle. We investigated fusion of additional DNA repair proteins to Cas9-CtIP as a method to bias DSB repair towards knockin and away from deleterious repair. While small molecules and genetic manipulations can be used to skew the balance of repair pathways in cells, such global perturbations can result in cell toxicity. Directly fusing repair proteins to Cas9 can obviate these toxicities by only modulating DNA repair locally at the target site.

For our study, repair molecules were chosen based on previous reporters highlighting their impact on DNA repair outcomes[28,32,33,34,23,27]. We found that N-terminal fusion of Rad52 and eRad18 improved the knockin precision of Cas9. Rad52 is a ssDNA-binding protein that

mediates DNA repair both through the single-strand annealing (SSA) pathway in a Rad51-independent manner, as well as through homologous recombination in a Rad51-depedent manner. Despite this however, in our study, Rad52 did not significantly impact the efficiency of knockin, whether in the presence or absence of CtIP. Instead, Rad52 fused to Cas9 alone reduced the frequency of knockout by 18%, and when combined with CtIP fusion led to an even greater 34% reduction. The *Saccharomyces cerevisiae* ortholog (ScRad52) may be more a potent knockin enhancer than the human variant that we used in this study, and it would be interesting to similarly characterize this related protein[26,35].

Unlike Rad52, fusion of eRad18 to Cas9 showed comparable increases in knockin rates with fusion of Cas9 to CtIP. It further resulted in 24% less knockout when combined with CtIP in compound fusions where Cas9 is flanked. Consistent with this effect, eRad18 was previously demonstrated to stimulate homology-dependent repair (HDR) by inhibiting 53BP1 localization to DSBs. While such donors can be challenging to construct, ssDNA donors can be synthesized commercially as single-stranded-oligodeoxynucleotide (ssODN) donors. However, unlike dsDNA donors which likely engage homology-dependent repair pathways, ssODN donors mediate editing through synthesis-dependent strand annealing (SDSA) and ssDNA incorporation (SI). Thus, depending on the cell context, different donors can offer improvements in knockin efficiency depending on the balance of DNA repair pathways in the target cell.

Importantly, our work presents a series of standardized platforms that can quantitatively and iteratively evaluate parameters that are critical for *in vivo* genome editing. The BFP-to-GFP conversion assay in HEK cells provides a high-throughput quantitative readout of not only editing efficiency (% GFP+ cells) but also the presence of unintended, deleterious edits (% BFP- cells). By simultaneously evaluating knockin and knockout rates, we identified combinations that optimized not only efficiency, but also precision. Knockin of a fluorescence cassette into the highly expressed *ActB* locus similarly enables direct quantification of efficiency at an endogenous gene locus. Furthermore, using a simple two-color donor system this assay can measure the rate of biallelic modification, another critical aspect of gene editing. We validated the correspondence of these phenotypic fluorescence outputs with genotype of edited cells using decomposition of Sanger sequence data. While this approach does not have the sampling depth of next-generation sequencing techniques, its low cost and low technical barrier make it an attractive method for many labs to evaluate the fidelity of gene editing approaches in their own genes and cells of interest. These *in vitro* assays enable high-throughput characterization of knockin reagents, from which the optima are selected for evaluation *in vivo*. Importantly, the *in utero electroporation* assay allows the *in vivo* delivery of the same plasmids that were screened *in vitro*, offering further continuity and standardization for reagent assessment, as well as iterative cycles of *in vitro* to *in vivo* optimization.

Ultimately, with the diversity of applications for gene editing and the inherent limitations of existing tools, it is necessary to pursue many parallel and alternative approaches. Thus, having standardized platforms for direct comparison of new reagents and novel combinations thereof, is essential to advance the field. Our study presents such an experimental workflow to aid in the developments towards the safe and effective use of *in vivo* gene editing for both basic research and human therapeutic benefit.

Acknowledgements

This work was supported by the High-Risk, High-Reward Research Program of the National Institutes of Health Common Fund under award number DP2MH122398. RRR was supported through the Cancer Biology T32 Training Program at the University of Maryland School of Medicine funded by the National Cancer Institute under award number T32CA154274. JI and SK were supported by the University of Maryland STAR-PREP Science Training for Advancing

Biomedical Research Postbaccalaureate Program funded by the National Institutes of Health under award number R25GM113262. We are grateful for the technical and instrumentation support of the University of Maryland School of Medicine Center for Innovative Biomedical Resources through the Confocal Imaging Facility, the Flow Cytometry Facility, the Genomics Facility, and the Biostatistics Shared Service.

References

1. Ho, B. X., Loh, S. J. H., Chan, W. K. & Soh, B. S. In vivo genome editing as a therapeutic approach. *Int. J. Mol. Sci.* **19,** (2018).
2. Hung, S. S. C., McCaughey, T., Swann, O., Pébay, A. & Hewitt, A. W. Genome engineering in ophthalmology: Application of CRISPR/Cas to the treatment of eye disease. *Prog Retin Eye Res* **53,** 1–20 (2016).
3. Li, Y., Glass, Z., Huang, M., Chen, Z.-Y. & Xu, Q. Ex vivo cell-based CRISPR/Cas9 genome editing for therapeutic applications. *Biomaterials* **234,** 119711 (2020).
4. Grade, S. & Götz, M. Neuronal replacement therapy: previous achievements and challenges ahead. *npj Regen. Med.* **2,** 29 (2017).
5. Henriques, D., Moreira, R., Schwamborn, J., Pereira de Almeida, L. & Mendonça, L. S. Successes and hurdles in stem cells application and production for brain transplantation. *Front. Neurosci.* **13,** 1194 (2019).
6. Bakondi, B. In vivo versus ex vivo CRISPR therapies for retinal dystrophy. *Expert Rev Ophthalmol* **11,** 397–400 (2016).
7. Bakondi, B. *et al.* In Vivo CRISPR/Cas9 Gene Editing Corrects Retinal Dystrophy in the S334ter-3 Rat Model of Autosomal Dominant Retinitis Pigmentosa. *Mol. Ther.* **24,** 556–563 (2016).
8. Cambria, E. *et al.* Translational cardiac stem cell therapy: advancing from first-generation to next-generation cell types. *npj Regen. Med.* **2,** 17 (2017).
9. Mikuni, T., Nishiyama, J., Sun, Y., Kamasawa, N. & Yasuda, R. High-Throughput, High-Resolution Mapping of Protein Localization in Mammalian Brain by In Vivo Genome Editing. *Cell* **165,** 1803–1817 (2016).
10. Suzuki, K. *et al.* In vivo genome editing via CRISPR/Cas9 mediated homology-independent targeted integration. *Nature* **540,** 144–149 (2016).
11. Willems, J. *et al.* ORANGE: A CRISPR/Cas9-based genome editing toolbox for epitope tagging of endogenous proteins in neurons. *PLoS Biol.* **18,** e3000665 (2020).
12. Gao, Y. *et al.* Plug-and-Play Protein Modification Using Homology-Independent Universal Genome Engineering. *Neuron* **103,** 583–597.e8 (2019).
13. Charpentier, M. *et al.* CtIP fusion to Cas9 enhances transgene integration by homology-dependent repair. *Nat. Commun.* **9,** 1133 (2018).
14. Engler, C., Kandzia, R. & Marillonnet, S. A one pot, one step, precision cloning method with high throughput capability. *PLoS One* **3,** e3647 (2008).
15. Duportet, X. *et al.* A platform for rapid prototyping of synthetic gene networks in mammalian cells. *Nucleic Acids Res.* **42,** 13440–13451 (2014).
16. Richardson, C. D. *et al.* CRISPR-Cas9 genome editing in human cells occurs via the Fanconi anemia pathway. *Nat. Genet.* **50,** 1132–1139 (2018).
17. Hsiau, T. *et al.* Inference of CRISPR Edits from Sanger Trace Data. *BioRxiv* (2018). doi:10.1101/251082
18. Saito, T. & Nakatsuji, N. Efficient gene transfer into the embryonic mouse brain using in vivo electroporation. *Dev. Biol.* **240,** 237–246 (2001).

19. Poulopoulos, A. *et al.* Subcellular transcriptomes and proteomes of developing axon projections in the cerebral cortex. *Nature* **565,** 356–360 (2019).
20. Kleinstiver, B. P. *et al.* High-fidelity CRISPR-Cas9 nucleases with no detectable genome-wide off-target effects. *Nature* **529,** 490–495 (2016).
21. Idoko-Akoh, A., Taylor, L., Sang, H. M. & McGrew, M. J. High fidelity CRISPR/Cas9 increases precise monoallelic and biallelic editing events in primordial germ cells. *Sci. Rep.* **8,** 15126 (2018).
22. Nakade, S. *et al.* Biased genome editing using the local accumulation of DSB repair molecules system. *Nat. Commun.* **9,** 3270 (2018).
23. Tran, N.-T. *et al.* Enhancement of precise gene editing by the association of cas9 with homologous recombination factors. *Front. Genet.* **10,** 365 (2019).
24. Maggio, I. & Gonçalves, M. A. F. V. Genome editing at the crossroads of delivery, specificity, and fidelity. *Trends Biotechnol.* **33,** 280–291 (2015).
25. Brinkman, E. K., Chen, T., Amendola, M. & van Steensel, B. Easy quantitative assessment of genome editing by sequence trace decomposition. *Nucleic Acids Res.* **42,** e168 (2014).
26. Shao, S. *et al.* Enhancing CRISPR/Cas9-mediated homology-directed repair in mammalian cells by expressing Saccharomyces cerevisiae Rad52. *Int. J. Biochem. Cell Biol.* **92,** 43–52 (2017).
27. Nambiar, T. S. *et al.* Stimulation of CRISPR-mediated homology-directed repair by an engineered RAD18 variant. *Nat. Commun.* **10,** 3395 (2019).
28. Jayavaradhan, R. *et al.* CRISPR-Cas9 fusion to dominant-negative 53BP1 enhances HDR and inhibits NHEJ specifically at Cas9 target sites. *Nat. Commun.* **10,** 2866 (2019).
29. Yao, X. *et al.* Homology-mediated end joining-based targeted integration using CRISPR/Cas9. *Cell Res.* **27,** 801–814 (2017).
30. Huertas, P. & Jackson, S. P. Human CtIP mediates cell cycle control of DNA end resection and double strand break repair. *J. Biol. Chem.* **284,** 9558–9565 (2009).
31. Shibata, A. *et al.* Factors determining DNA double-strand break repair pathway choice in G2 phase. *EMBO J.* **30,** 1079–1092 (2011).
32. Paulsen, B. S. *et al.* Ectopic expression of RAD52 and dn53BP1 improves homology-directed repair during CRISPR-Cas9 genome editing. *Nat. Biomed. Eng.* **1,** 878–888 (2017).
33. Tang, J. *et al.* Acetylation limits 53BP1 association with damaged chromatin to promote homologous recombination. *Nat. Struct. Mol. Biol.* **20,** 317–325 (2013).
34. An, L. *et al.* RNF169 limits 53BP1 deposition at DSBs to stimulate single-strand annealing repair. *Proc. Natl. Acad. Sci. USA* **115,** E8286–E8295 (2018).
35. Di Primio, C., Galli, A., Cervelli, T., Zoppè, M. & Rainaldi, G. Potentiation of gene targeting in human cells by expression of Saccharomyces cerevisiae Rad52. *Nucleic Acids Res.* **33,** 4639–4648 (2005).